MALAYSIAN JOURNAL OF MICROSCOPY

Journal homepage: https://malaysianjournalofmicroscopy.org

RESEARCH ARTICLE

SYNTHESIS OF BLACK TEA STALK BASED ACTIVATED CARBON VIA CHEMICAL ACTIVATION FOR SCAVENGING ZN(II) IONS IN AQUEOUS SOLUTION

Erniza Mohd Johan Jaya[1], Mohamad Firdaus Mohamad Yusop[1], Azduwin Khasri[2], Mohd Azmier Ahmad[1*]

[1]School of Chemical Engineering, Engineering Campus, Universiti Sains Malaysia, 14300 Nibong Tebal, Pulau Pinang, Malaysia.

[2]Faculty of Chemical Engineering & Technology, Kompleks Pusat Pengajian Jejawi 3, Universiti Malaya Perlis (UNIMAP), 02600 Arau, Perlis, Malaysia.

Abstract. Activated carbon (AC) synthesized from biomass is an environmentally friendly water purification method, as it provides a green solution that harnesses renewable resources to efficiently adsorb pollutants. Zinc ions (Zn(II)) are common pollutant found in wastewater, posing a risk to the ecosystem. Consequently, the objective of this research is to manufacture AC from black tea stalks (TSAC) to adsorb Zn(II) ions. The TSAC was prepared through chemical activation method using potassium hydroxide (KOH) at a ratio of 1:1. Characterization of the pore structure gave BET surface area of 892.56 m^2/g and a total pore volume of 0.31 cm^3/g. These properties provide a large surface area and pore volume to trap the Zn(II) ions. Scanning electron microscopy (SEM) analysis of the precursor displayed a dense surface and lack of pore structure. Conversely, the TSAC revealed a surface that was notably porous. The equilibrium study examined the effects of initial Zn(II) concentration (5 to 30 mg/L), contact time (1-8 hours), and solution temperature (30, 45 and 60 °C), with a fixed TSAC dosage of 0.20g. The results reveal that as the Zn(II) concentration increases, there is an increase in adsorption uptake while the corresponding percentage removal decreases. The optimal Zn(II) uptake by TSAC occurs at a solution temperature of 60 °C. Isotherm studies indicate that the Zn(II)-TSAC adsorption system adheres to the Freundlich model, with maximum monolayer adsorption capacity (Q_m) of 28.74 mg/g. In kinetic studies, the pseudo-first-order (PFO) model is the most suitable for describing the Zn(II)-TSAC adsorption system. Boyd plot analysis indicates that the controlling factor is film diffusion. The application of KOH chemical treatment has resulted in the formation of well-defined pores, thereby improving the TSAC ability to adsorb Zn(II) ions.

Keywords: Activated carbon, chemical activation, adsorption, Zn(II).

Article Info

Received 5 December 2023
Accepted 5 October 2024
Published 6 December 2024

***Corresponding author: chazmier@usm.my**

ISSN: 1823-7010, eISSN: 2600-7444

1. INTRODUCTION

Heavy metals in water can be a cause for concern due to their potential impact on both human health and the environment. Heavy metals persist in water bodies, accumulating in sediments and aquatic organisms. Their toxicity and high solubility lead to bioaccumulation and biomagnification, posing significant environmental hazards. Bioaccumulation threatens the food chain as heavy metals accumulate in smaller organisms and magnify in larger predators through biomagnification. This results in higher concentrations of heavy metals at each trophic level, posing significant risks to wildlife and humans. Heavy metals are associated with health concerns such as kidney and liver damage, skin irritation, nerve tissue impairment, and the development of cancers in vital organs like the skin, bladder, and lungs [1]. Among the widely employed heavy metals in industries, zinc stands out as one of the most popular and extensively utilized. Zinc is valued for its excellent corrosion resistance, making it ideal for galvanizing steel. It's also used in alloys like brass and bronze for their strength and durability, and in batteries for efficient energy storage [2]. However, its presence in wastewater and industrial effluents can pose environmental and health risks. Regulatory agencies, such as the World Health Organization (WHO), set a maximum contaminant level of 3 mg/L for zinc in drinking water to safeguard public health and prevent potential adverse effects [3]. The presence of heavy metals in water bodies is a complex environmental issue with multifaceted origins. Industrial activities, urbanization, and agricultural practices are primary contributors to the contamination of water bodies with heavy metals. There are many recent studies that highlight the current situation of heavy metal pollution, revealing alarming levels of contaminants such as cadmium, lead, and zinc, as well as emphasizing the need for remediation efforts to address the environmental and health risks associated with heavy metal pollution [4].

Adsorption, which involves the binding of heavy metal ions to the surface of the adsorbent material, is considered an effective method for treating wastewater. This approach presents benefits such as straightforward operation, durability in toxic conditions, and the possibility of reusing the adsorbent through the renderability process [5]. Various adsorbents, such as hydrochar, biochar, clay, and biosorbents, are utilized in the adsorption process. Among these, activated carbon (AC) stands out as a widely recognized adsorbent, where coal is the commonly used precursor due to its abundance and cost-effectiveness. However, the environmental impact, including carbon emissions and other pollutants, has prompted a search for alternative and renewable precursors. Transitioning from coal to biomass as a precursor for AC represents a significant shift towards a more environmentally friendly approach in AC production. Examples of biomass precursors include date seeds [6], jackfruit peel [5], durian seed [7], corncob [8], and so on. In literature, biomass-based AC was succeeded in adsorbing various types of pollutants in wastewater [9-10]. This study chose tea stalks as a precursor for AC production because they are a sustainable, abundant byproduct of tea production, rich in carbon, and naturally porous. The production of the AC involves a series of steps. The first step involves the carbonization process, where the precursor is pyrolyzed at a high temperature under an inert atmosphere. Carbonization is a crucial step in the production of AC, transforming carbon-rich precursors into a carbonized form. The second step is the activation step, which can be categorized into physical activation, chemical activation, and physicochemical activation.

In this work, chemical activation is employed, utilizing potassium hydroxide (KOH) as the activating agent. KOH reacts with the carbon material to create a network of micropores and mesopores, increasing the surface area and enhancing the material’s adsorption capacity. The objectives of this study are to synthesize AC from black tea stalks using chemical activation, characterize its physical, chemical, and morphological properties, and evaluate its efficiency in adsorbing Zn(II) ions from aqueous solutions.

2. MATERIALS AND METHODS

2.1 Materials

The tea stalk was acquired from a morning market in Seberang Jaya, Pulau Pinang. The potassium hydroxide, KOH pellet (85 %), and hydrochloric acid, HCl (37 % assay) were supplied by Sigma-Aldrich. Metal salts of $Zn(NO_3)_2$ and NaOH, both of analytical reagent grade, were procured from Sigma-Aldrich and Merck Company. MOX Gases Berhad, Malaysia, furnished nitrogen gas (N_2) and carbon dioxide gas (CO_2) with a purity of 99.99 %.

2.2 TSAC Preparation

The tea stalk precursor underwent a thorough rinse with distilled water and was subsequently dried in an oven for approximately 48 hours. Following this, the precursor underwent carbonization at 550 °C for 2 hours under a flow of N_2 gas at a rate of 150 cm^3 min^{-1}, resulting in the formation of char. After carbonization, the carbonized material was cooled down with inert gas (N_2) to prepare it for subsequent activation treatment. This rapid cooling method prevents oxidation and helps maintain the specific properties of the char. The ensuing char was then impregnated with KOH at a ratio of 1:1 by weight for 24 hours. The impregnation ratio selected ensures that there is enough KOH to fully interact with the carbon, promoting the formation of an extensive pore network without causing excessive burn-off of the carbon, which could reduce the yield of activated carbon since the potassium hydroxide (KOH) is a strong activating agent. KOH promotes the formation of pores by etching away parts of the carbon matrix, increasing the surface area, and creating a porous structure. Subsequently, the impregnated sample underwent multiple washes with deionized water to remove any residual KOH and other impurities. The pH of the washed solution was checked periodically until it reached 7. This step is crucial because a neutral pH minimizes the risk of further chemical reactions on the surface of the activated carbon that could degrade its structure and effectiveness. If the AC is left too acidic or alkaline, it could undergo further reactions that might reduce its mechanical stability or alter its pore structure, diminishing its adsorption capacity over time. Neutral pH ensures that the AC remains chemically stable during storage and use. The resulting wet sample, referred to as TSAC, was dried in an oven for 24 hours before being stored in an airtight container.

2.3 Characterization Methods

The study delved into the physicochemical attributes of the samples, encompassing an examination of surface area (utilizing BET and mesopore measurements), pore size, and pore volume. These analyses were carried out using a Micromeritics volumetric adsorption analyzer (ASAP 2010). In addition, elemental analysis was performed using the Perkin Elmer Series II 2400 from the United States. To gain insights into the surface morphology, scanning electron microscopy (SEM) images were captured and documented using the Quanta 450 FEG instrument from the Netherlands.

2.4 Study of Equilibrium

The equilibrium study examined the uptake of Zn(II) while taking into account three variables: initial concentration of Zn(II), contact time, and solution temperature. To investigate the impact of Zn(II) initial concentration, Erlenmeyer flasks were set up with six different concentrations (5, 10, 15, 20, 25 and 30 mg/L). These flasks were then placed in a water bath shaker operating at a rotation speed of 80 rpm. Throughout the experiments, the solution volume, TSAC weight, and solution temperature were kept constant at 200 mL, 0.20 g, and 30 °C, respectively, while maintaining a constant solution pH. To explore the influence of solution temperature, a Zn(II) solution with an initial concentration of 30 mg/L was used at three distinct temperatures (30, 45 and 60 °C), with other parameters held constant. Upon achieving equilibrium, the adsorbate solution underwent analysis using a UV-Vis spectrophotometer (Agilent Cary 60, USA). The Zn(II) uptakes and their corresponding removal percentages were calculated using the following equations, respectively:

$$q_e = \frac{(C_o - C_e)V}{W} \quad (1)$$

$$\%\ Removal = \frac{C_o - C_e}{C_o} \text{ X } 100\% \quad (2)$$

where qe is the Zn(II) adsorption uptakes at equilibrium (mg/g), Co denotes as concentration of Zn(II) at initial (mg/L), Ce stands for the concentration of Zn(II) at equilibrium (mg/L), W indicates the weight of TSAC (g) and V is the volume of Zn(II) solution (mL).

2.5 Study of Isotherm

The isotherm study involved fitting the adsorption data to three models: Langmuir, Freundlich, and Temkin. Their respective formulas are provided as follows:

Langmuir [11]:

$$q_e = \frac{Q_m K_L C_e}{1 + K_L C_e} \quad (3)$$

Freundlich [12]:

$$q_e = K_F C_e^{1/n_F} \quad (4)$$

Temkin [13]:

$$q_e = \frac{RT}{B} \ln (AC_e) \quad (5)$$

where Q_m is the Langmuir adsorption uptakes (mg/g), K_L is the constant of Langmuir that relates to the adsorption capacity (mg/g), and K_F stands for Freundlich constant ((mg/g)(L/mg)$^{1/n}$). n_F (dimensionless) shows the ferocity of the surface heterogeneity. A and B refer to the Temkin constants.

2.6 Study of Kinetic

The kinetics investigation adhered to a procedure similar to the equilibrium study, involving the measurement of Zn(II) concentration at designated time intervals. Six solutions of Zn(II) ranging from 5 to 50 mg/L, a TSAC weight of 0.20 g, a solution temperature of 30 °C, an initial pH of the solution, and a rotation speed of 80 rpm were employed. The kinetic data underwent fitting to three models: pseudo-first order (PFO), pseudo-second order (PSO), and Boyd plot. The respective equations for these models are as follows:

Pseudo-first order (PFO) [14]:

$$\ln(q_e - q_t) = \ln q_e - k_1 t \quad (6)$$

Pseudo-second order (PSO) [14]:

$$\frac{t}{q_t} = \frac{1}{k_2 q_e^2} + \frac{t}{q_e} \quad (7)$$

Boyd plot [15]:

$$B_t = -0.4977 - ln \left(1 - \frac{q_t}{q_e}\right) \quad (8)$$

where k_1 and k_2 represent the rate constants for the pseudo-first order (PFO) and pseudo-second order (PSO) models, respectively, and B_t is denoted as the Boyd number. The selection of the most appropriate model describing the adsorption data was determined using the root mean square error (RMSE), which is calculated using the following formula:

$$RMSE = \sqrt{\frac{1}{n-1}\sum_{n=1}^{n}\left(q_{e,exp,n} - q_{e,cal,n}\right)^2} \quad (9)$$

where n refers to the number of points.

3. RESULTS AND DISCUSSION

3.1 Physical, Chemical, and Morphological Characterization

The effectiveness of AC hinges on its surface area and pore features. AC's expansive surface area offers numerous active sites for adsorption, attracting and retaining metal ions on its surface. This extensive surface ensures a higher capacity to adsorb impurities from gases or liquids. Equally vital are the pore characteristics, encompassing micropores, mesopores, and macropores. This varied pore structure caters to a broad spectrum of molecular sizes, enhancing AC's capability to adsorb various substances. Table 1 outlines the surface area and pore characteristics of the samples. The precursor displayed a low BET surface area of 1.05 m^2/g, and details regarding mesopores surface area, total pore volume, and average pore diameter were not available. Following the carbonization and activation process, TSAC exhibited a substantial increase in BET surface area (892.56 m^2/g), mesopore surface area (712.49 m^2/g), and total pore volume (0.31 cm^3/g). The average pore diameter for TSAC also expanded from 1.58 nm (micropores) in char to 2.37 nm (mesopores) in TSAC, a result of the KOH chemical treatment. The KOH activation showed an effective enlargement of pore structures, transforming micropores into mesopores by etching and widening the carbon matrix. This phenomenon mirrors observations in the production of teak wood-based activated carbon, where KOH facilitated pore development from 2.64 nm to 2.85 nm, highlighting the method's efficacy in enhancing pore structure and adsorption capacity [16].

Table 1: Surface area and pore characteristics of the tea stalk precursor, char and TSAC adsorbent

Sample	BET surface area (m^2/g)	Mesopores surface area (m^2/g)	Total pore volume (cm^3/g)	Average pore diameter (nm)
Precursor	1.05	-	-	-
Char	337.16	246.87	0.13	1.58
TSAC	892.56	712.49	0.31	2.37

Examining the proximate and elemental analyses is crucial for comprehending and enhancing the properties of AC. Proximate analysis furnishes vital details about the major components of AC, impacting its combustion behaviour, stability, and overall performance. On the flip side, elemental analysis explores the elemental composition, uncovering the presence of carbon, hydrogen, nitrogen, sulphur, and oxygen. The proportions and percentages of these elements play a role in shaping AC's chemical reactivity, adsorption capacities, and thermal stability. Table 2 presents the outcomes of proximate and elemental analyses for the samples. The precursor exhibited a noteworthy elemental carbon (C) content of 48.71 %, a relatively high value. Upon completion of carbonization and activation, the carbon content in TSAC significantly increased to 81.44 %. Conversely, other elements, namely hydrogen (H), sulfur (S), and nitrogen plus oxygen (N + O), experienced reductions, decreasing from

7.41 % to 6.14 %, 1.03 % to 0.07 %, and 42.85 % to 12.32 %, respectively. Proximate analysis indicated a substantial decrease in moisture and volatile matter, reducing from 4.12 % to 2.14 % and from 62.87 % to 18.49 %, respectively. This decrease was attributed to the efficiency of the carbonization and activation processes in eliminating water molecules and volatile components like lignin, cellulose, hemicellulose, and tar through evaporation and thermal cracking processes. The percentage of fixed carbon witnessed a significant increase from 27.15 % to 77.89 %. Given that fixed carbon contributes to the matrix structure of TSAC, a higher fixed carbon value was considered advantageous [16]. Ultimately, the ash percentage in the precursor and TSAC was determined to be 5.86 % and 1.48 %, respectively. The low ash percentage is a desirable characteristic of AC, as ash lacks pores and does not contribute to the adsorption process [5].

Table 2: Proximate and elemental analysis of tea stalk precursor and TSAC adsorbent

	Proximate analysis (%)				Elemental analysis (%)			
Samples	**Moisture**	**Volatile matter**	**Fixed carbon**	**Ash**	**C**	**H**	**S**	**(N+O)**
Precursor	4.12	62.87	27.15	5.86	48.71	7.41	1.03	42.85
TSAC	2.14	18.49	77.89	1.48	81.44	6.14	0.07	12.35

Scanning electron microscopy (SEM) images are pivotal in deciphering the structure of AC. These high-resolution images offer a detailed visualization of the surface morphology, porosity, and particle size distribution of AC. Grasping these structural aspects is paramount, as they directly influence the adsorption efficiency, surface area, and overall performance of AC. In Figure 1(a), the surface of the precursor exhibited a dense and pore-lacking appearance, in line with expectations attributed to the presence of components like lignin, cellulose, hemicellulose, and tar. Conversely, in Figure 1(b), the surface of TSAC displayed heightened porosity with numerous vacant cavities. Initially, these spaces were filled with volatile matter and moisture components, which later evaporated and escaped from the sample during the carbonization process. The subsequent chemical activation process, involving the penetration of KOH deep into the sample, contributed to the formation of pores.

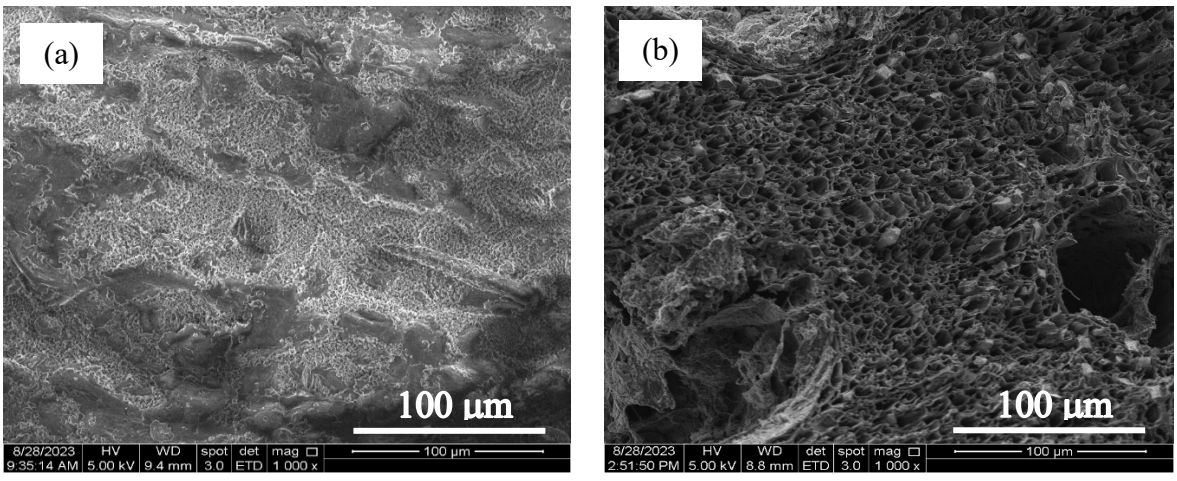

Figure 1: SEM images of (a) Dense surface of the tea stalk precursor, and (b) Porous structure of TSAC after carbonization and activation process

3.2 Adsorption Equilibrium

3.2.1 Effect of contact time and Zn(II) initial concentration

Figure 2(a) depicts the Zn(II) adsorption uptakes by TSAC at various concentrations over time, while Figure 2(b) illustrates the percentage removal of Zn(II) for different initial concentrations over time. As observed in Figure 2(a), with an increase in the initial concentration of Zn(II) from 5 to 30 mg/L, the adsorption uptakes of Zn(II) elevate from 4.98 to 21.45 mg/g. This observed trend indicates that at higher initial concentrations of Zn(II), a greater number of elements are present in the solution, thereby enhancing the capacity for Zn(II) adsorption by TSAC. Moreover, higher initial concentrations result in a more significant mass transfer driving force, overcoming the mass transfer resistance between adsorbate ions in the bulk and solid phases. According to Figure 2(b), with an increase in the initial concentration of Zn(II) from 5 to 30 mg/L, the percentage removal of Zn(II) decreased from 99.60 % to 71.50 %. This observed pattern implies that higher initial concentrations of Zn(II) correspond to a higher ratio of Zn(II) elements to available sites. While this leads to increased uptake, it concurrently results in a lower percentage of removal. Conversely, lower initial concentrations exhibit the opposite trend, demonstrating a lower adsorption uptake and higher percentage removal based on the concentration of Zn(II) in the system [17]. For the effects of contact time, adsorption equilibrium was observed to be achieved after 6 hours for higher Zn(II) ion concentrations (15, 20, 25, and 30 mg/L), while for lower concentrations (5 and 10 mg/L), equilibrium was reached at 3 hours. The equilibrium point indicates that the maximum adsorption capacity of the TSAC for Zn(II) has been achieved. Any additional contact time beyond this point may not result in a significant increase in the amount of Zn(II) ions adsorbed as the active sites on the TSAC become saturated.

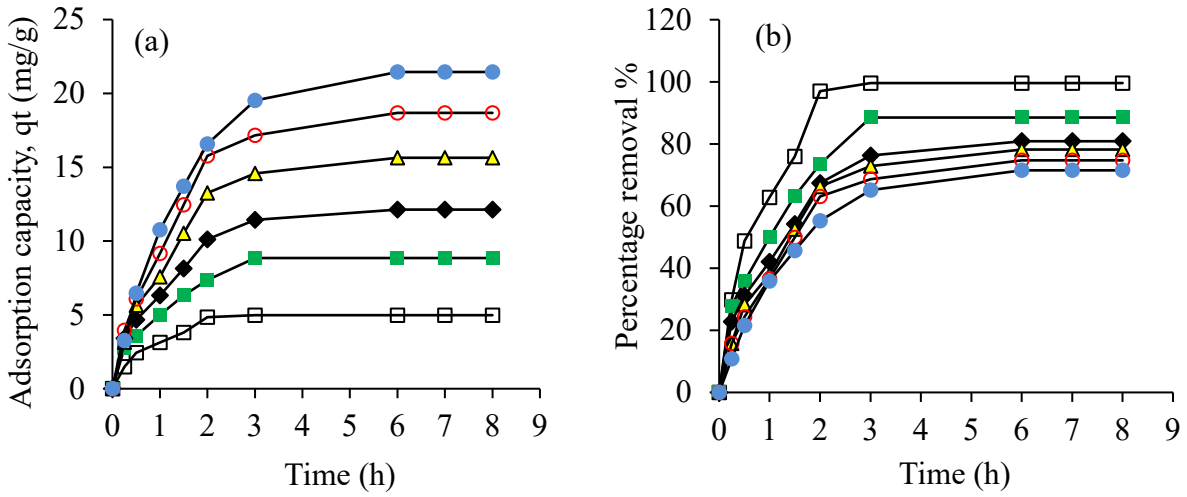

Figure 2: Plots of (a) Zn(II) uptakes against time and (b) percentage removal of Zn(II) against time at different initial concentration

3.2.2 Effect of solution temperature

In Figure 3, the graphs illustrate the relationship between Zn(II) adsorption uptakes and varying solution temperatures. It was observed that with an increase in the solution temperature from 30 to 60 °C, the adsorption uptakes of Zn(II) also increased, rising from 21.45 to 25.19 mg/g. This observation indicates that the adsorption process of Zn(II) is more favourable at elevated solution temperatures, suggesting an endothermic nature to the process.

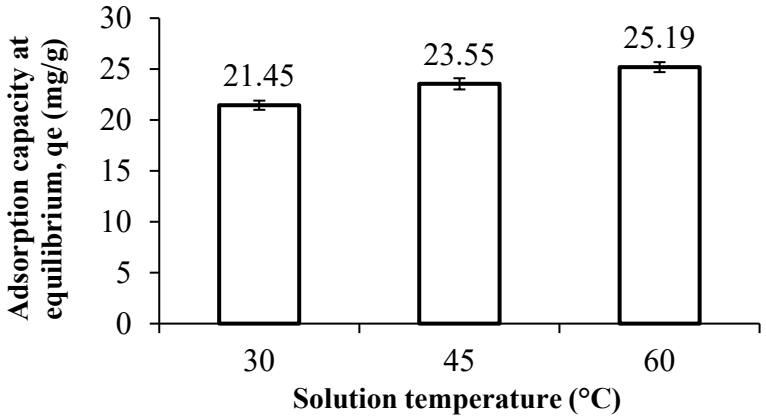

Figure 3: Plot on adsorption of Zn(II) uptakes against solution temperatures

3.3 Adsorption Isotherm

Investigations into isotherms in adsorption are crucial, offering a thorough understanding of the correlation between the quantity of adsorbate and its concentration on the adsorbent's surface. Through the plotting of adsorption isotherms that portray this equilibrium relationship under specific conditions, researchers glean insights into the adsorption mechanism, capacity, and surface characteristics of the adsorbent material. Figure 4 displays the isotherm plots associated with the Langmuir, Freundlich, and Temkin models, while Table 3 provides a synopsis of the isotherm parameters for the Zn(II)-TSAC adsorption system at 30 °C. The data suggests a close alignment of the Freundlich model with the observed behaviour, as indicated by the lowest RMSE of 1.43. This implies that Zn(II) ions establish multilayer coverage on the TSAC surface. Additionally, the Freundlich model is found to be the most fitting for other adsorption systems. The heterogeneity factor, represented as n_F and determined to be 2.63 for Zn(II)-TSAC, falls within the range of 1 to 10. This value suggests that the studied adsorption system is deemed favourable [16].

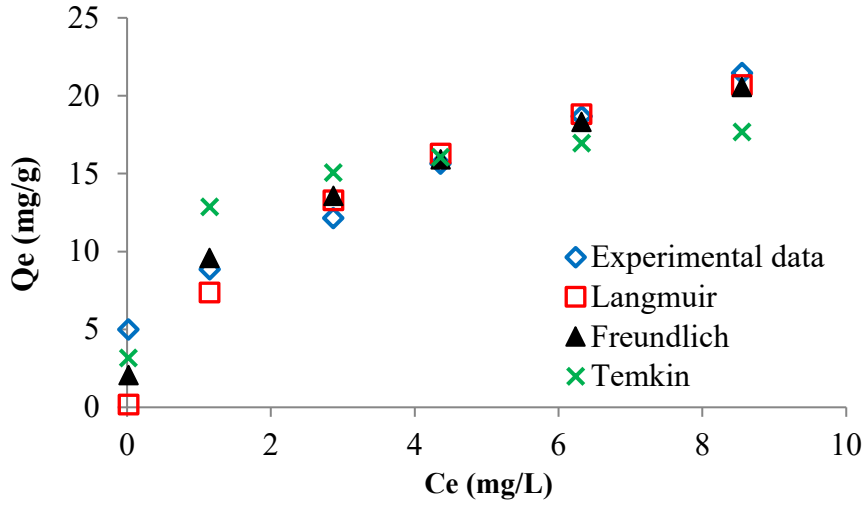

Figure 4: Isotherm plots of Langmuir, Freundlich and Temkin for Zn(II)-TSAC adsorption system at 30 °C

Table 3: Isotherm parameters for Zn(II)-TSAC adsorption system at 30 °C

Zn(II)-TCAC	
Langmuir	
Q_m (mg/g)	28.74
K_L (L/mg)	0.30
RMSE	2.15
Freundlich	
n_F	2.63
K_F (mg/g)(L/mg)$^{1/n}$	9.09
RMSE	1.43
Temkin	
B (L/mg)	2.39
A (L/mg)	187.80
RMSE	2.75

3.4 Adsorption Kinetic and Mechanism Study

The kinetics of adsorption are pivotal in comprehending and refining adsorption processes, providing valuable insights into the speed at which adsorption unfolds over time. Through the study of adsorption kinetics, researchers can discern the mechanisms and pathways involved in the interaction between the adsorbate and the adsorbent material. Figures 5(a) and (b) display the kinetic plots for PFO and PSO in the Zn(II)-TSAC system, respectively.

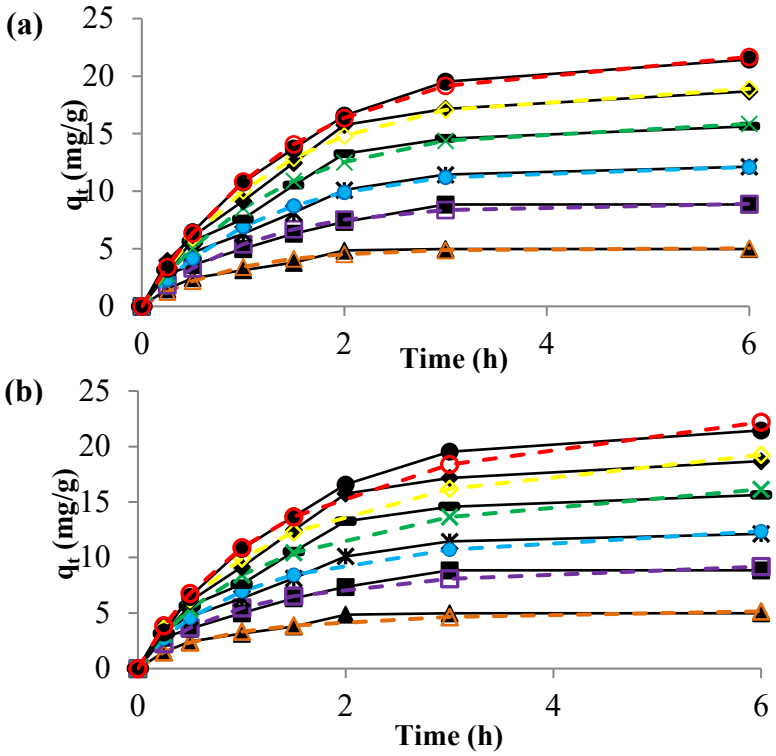

Figure 5: Kinetic plots for (a) PFO and (b) PSO for Zn(II)-TSAC adsorption system at 30 °C

Table 4 provides a summary of the kinetic parameters. The PFO kinetic model emerged as the most suitable fit for the adsorption system, supported by the lowest RMSE of 0.48. As the initial concentration of Zn(II) increased from 5 to 50 mg/L, the reaction rate (k1) decreased from 1.14 g mg^{-1}

min^{-1} to 0.68 g mg^{-1} min^{-1}. This decrease can be attributed to the higher abundance of Zn(II) ions in the solution at elevated initial concentrations. The heightened concentration amplified the competition among these elements for adsorption by TSAC, intensifying the competition and ultimately resulting in a lower reaction rate [18].

Table 4: Kinetic parameters for Zn(II)-TSAC adsorption system at 30 °C

Initial adsorbates concentration (mg/L)		q_e, exp (mg/g)	Pseudo-first order			Pseudo-second order		
			q_e, cal (mg/g)	k_1 (min^{-1})	RMSE	q_e, cal (mg/g)	k_2 (g mg^{-1} min^{-1})	RMSE
Zn(II)	5	4.98	5.05	1.14	0.27	5.78	0.2356	0.28
	10	8.85	8.94	0.92	0.51	10.62	0.0999	0.56
	15	12.13	12.19	0.84	0.62	14.64	0.0620	0.52
	20	15.64	16.02	0.76	0.60	19.76	0.0377	0.57
	25	18.68	19.12	0.75	0.64	23.72	0.0302	0.68
	30	21.45	22.05	0.68	0.26	28.01	0.0227	0.62
	Average				0.48			0.54

Figure 6 presents Boyd plots depicting the Zn(II)-TSAC adsorption system at 30 °C. The analysis reveals that film diffusion acts as the controlling factor in the rate-limiting stages for all the investigated adsorption systems. This conclusion is drawn from the observation that these plots do not intersect at the origin.

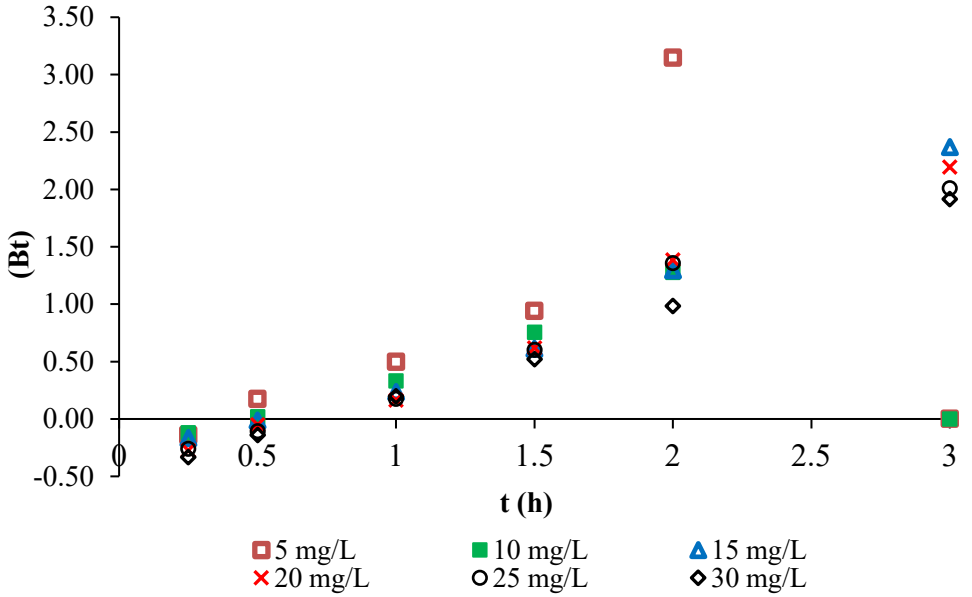

Figure 6: Boyd plot for Zn(II)-TSAC adsorption systems at 30°C

4. CONCLUSIONS

This study highlights the significant potential of TSAC as a highly effective biomass-based adsorbent for the removal of Zn(II) ions from wastewater via the adsorption process. Through effective chemical activation using KOH, the tea stalk-based activated carbon (TSAC) was successfully developed and exhibited a remarkable Zn(II) removal capability, achieving a maximum adsorption capacity (Q_m) of 28.74 mg/g. The TSAC exhibited noteworthy features, including a high BET surface area (892.56 m^2/g), mesopore surface area (712.49 m^2/g), total pore volume (0.31 cm^3/g), and fixed carbon content (77.89 %). In the equilibrium study, an increase in the initial concentration of Zn(II)

from 5 to 30 mg/L led to higher adsorption uptakes but a decrease in percentage removal. To further enhance the percentage removal and minimize the likelihood of fouling, surface modifications of the TSAC are recommended to address these issues. The highest Zn(II) uptake occurred at a solution temperature of 60 °C (25.19 mg/g). The adsorption data for Zn(II)-TSAC demonstrated a good fit with the Freundlich isotherm model, and the PFO kinetic model proved most effective. Analysis of the rate-determining step through Boyd plots revealed the crucial role of film diffusion. Overall, the TSAC produced exhibited exceptional properties, making it an effective and highly suitable adsorbent for the treatment of Zn(II)-containing wastewater.

Acknowledgments

This research was supported by the Ministry of Higher Education Malaysia through the Fundamental Research Grant Scheme (project code: FRGS/1/2021/TK0/USM/01/3).

Author Contributions

All authors contributed toward data analysis, drafting, and critically revising the paper and agree to be accountable for all aspects of the work.

Disclosure of Conflict of Interest

The authors have no disclosures to declare.

Compliance with Ethical Standards

The work adheres to the ethical standards, ensuring that all experimental procedures and methodologies were conducted with integrity and respect for ethical guidelines.

References

[1] Iqbal, M. O. & Yahya, E. B. (2021). In vivo assessment of reversing aminoglycoside antibiotics nephrotoxicity using Jatropha mollissima crude extract. *Tissue and Cell,* 72, 101525.

[2] Azeez, N. R., Salih, S. S., Kadhom, M., Mohammed, H. N. & Ghosh, T. K. (2024). Enhanced termination of zinc and cadmium ions from wastewater employing plain and chitosan-modified mxenes: synthesis, characterization, and adsorption performance. *Green Chemical Engineering,* 5(3), 339-347.

[3] Sergio, B. M., Jaimes, R., Borysow, W., Gomes, O. & Salcedo, W. (2017). Portable multispectral colorimeter for metallic ion detection and classification. *Sensors*, 17, 1730.

[4] Sharma, R., Agrawal, P. R., Kumar, R., Gupta, G. & Ittishree. (2021). Chapter 4 - Current Scenario of Heavy Metal Contamination in Water. In *Contamination of Water*, Ed. Ahamad, A., Siddiqui, S. I., & Singh, P. (Academic Press), pp. 49-64.

[5] Yusop, M. F. M., Abdullah, A. Z. & Ahmad, M. A. (2023). Adsorption of remazol brilliant blue R dye onto jackfruit peel based activated carbon: Optimization and simulation for mass transfer and surface area prediction. *Inorganic Chemistry Communications,* 158, 111721.

[6] Said, B., Bacha, O., Rahmani, Y., Harfouche, N., Kheniche, H., Zerrouki, D., Belkhalfa, H. & Henni, A. (2023). Activated carbon prepared by hydrothermal pretreatment-assisted chemical activation of date seeds for supercapacitor application. *Inorganic Chemistry Communications,* 155, 111012.

[7] Ahmad, M. A., Hamid, S. R. A., Yusop, M. F. M. & Aziz, H. A. (2017). Optimization of microwave-assisted durian seed based activated carbon preparation conditions for methylene blue dye removal. In Proceedings of the International Conference of Global Network for Innovative Technology and Awam International Conference in Civil Engineering (Ignite-Aicce'17), Malaysia, 8–9 August 2017.

[8] Abdillah, N., Mohamad Yusop, M. F., Mokhtar Kamal, N. H. & Azmier Ahmad, M. (2023). Single-stage microwave-irradiated activated carbon from corncob for ammonia nitrogen removal: Batch, attraction mechanism and regeneration studies. *Inorganic Chemistry Communications,* 158, 111672.

[9] Yusop, M. F. M., Mohd Johan Jaya, E., Mohd Din, A. T., Bello, O. S. & Ahmad, M. A. (2022). Single-Stage Optimized Microwave-Induced Activated Carbon from Coconut Shell for Cadmium Adsorption. *Chemical Engineering & Technology,* 45(11), 1943-1951.

[10] Firdaus, M. Y. M., Abdullah, A. Z. & Ahmad, M. A. (2024). Amoxicillin adsorption from aqueous solution by Cu(II) modified lemon peel based activated carbon: Mass transfer simulation, surface area prediction and F-test on isotherm and kinetic models. *Powder Technology,* 438, 119589.

[11] Mechati, F., Djilani, C., Bougdah, N., Messikh, N., Boussaha, E., Moumen, A., Bouchalta, C. & Medjram, M. S. (2023). Adsorption of methylene blue onto activated carbon prepared under N2/microwave radiation supported cobalt: kinetics, isotherms, and thermodynamics studies. *Desalination and Water Treatment,* 284, 288-300.

[12] Bouchelkia, N., Tahraoui, H., Amrane, A., Belkacemi, H., Bollinger, J.-C., Bouzaza, A., Zoukel, A., Zhang, J. & Mouni, L. (2023). Jujube stones based highly efficient activated carbon for methylene blue adsorption: Kinetics and isotherms modeling, thermodynamics and mechanism study, optimization via response surface methodology and machine learning approaches. *Process Safety and Environmental Protection,* 170, 513-535.

[13] Lahuri, A. H., Rahim, A. A., Nordin, N., Adnan, R., Jaafar, N. F. & Taufiq-Yap, Y. H. (2023). Comparative studies on adsorption isotherm and kinetic for CO_2 capture using iron oxide impregnated activated carbon. *Catalysis Today,* 418, 114111.

[14] Tünay, S., Köklü, R. & İmamoğlu, M. (2022). Removal of diclofenac, ciprofloxacin and sulfamethoxazole from wastewater using granular activated carbon from hazelnut shell: isotherm, kinetic and thermodynamic studies. *Desalination and Water Treatment,* 277, 155-168.

[15] Vega, M. F., Díaz-Faes, E. & Barriocanal, C. (2024). Kinetic and mechanistic study of CO2 adsorption on activated hydrochars. *Journal of CO2 Utilization,* 81, 102716.

[16] Firdaus, M. Y. M., Aziz, A. & Azmier Ahmad, M. (2022). Conversion of teak wood waste into microwave-irradiated activated carbon for cationic methylene blue dye removal: Optimization and batch studies. *Arabian Journal of Chemistry,* 15(9), 104081.

[17] Ahmad, M. A., Eusoff, M. A., Oladoye, P. O., Adegoke, K. A. & Bello, O. S. (2021). Optimization and batch studies on adsorption of Methylene blue dye using pomegranate fruit peel based adsorbent. *Chemical Data Collections,* 32, 100676.

[18] Firdaus, M. Y. M., Tamar Jaya, M. A., Idris, I., Abdullah, A. Z. & Ahmad, M. A. (2023). Optimization and mass transfer simulation of remazol brilliant blue R dye adsorption onto meranti wood based activated carbon. *Arabian Journal of Chemistry,* 16(5), 104683.